Journal of ELECTRONIC MATERIALS, Vol. 49, No. 4, 2020
https://doi.org/10.1007/s11664-019-07935-8

Enhanced Thermoelectric Performance of Polythiophene/Carbon Nanotube-Based Composites

X.Y. JIANG,[1] Q.K. ZHANG,[1] S.P. DENG,[1] B. ZHOU,[1] B. WANG,[1] Z.Q. CHEN ,[1,3] N. QI,[1,4] and X.F. TANG[2]

1.—Hubei Nuclear Solid Physics Key Laboratory, Department of Physics, Wuhan University, Wuhan 430072, China. 2.—State Key Laboratory of Advanced Technology for Materials Synthesis and Processing, Wuhan University of Technology, Wuhan 430070, China. 3.—e-mail: chenzq@whu.edu.cn. 4.—e-mail: ningqi@whu.edu.cn

Binary polythiophene/multiwalled carbon nanotube (PTh/MWCNT) and ternary PTh/SnSe/MWCNT composites with different weight proportions have been successfully prepared by solution mixing, ultrasonic dispersion, and mechanical ball milling. The morphology, microstructure, and thermal stability of all the samples were studied by x-ray diffraction analysis, Fourier-transform infrared spectroscopy, field-emission scanning electron microscopy, and thermogravimetric analysis. The electrical conductivity of both the binary PTh/MWCNT and ternary PTh/SnSe/MWCNT composites was increased by nearly five orders of magnitude compared with pure PTh across the whole measurement temperature range. However, the Seebeck coefficient at room temperature decreased sharply from $453.4\,\mu VK^{-1}$ for pure PTh to $11-20\,\mu VK^{-1}$ for the composites. The thermal conductivity of all the composites was lower than $0.6\ Wm^{-1}K^{-1}$, being slightly higher than that of pure PTh. As a result, the ZT values of all the composites were much higher than that of pure PTh (0.032×10^{-4}), reaching 1.3×10^{-4} and 1.62×10^{-4} at room temperature for the binary PTh/MWCNT and ternary PTh/SnSe/MWCNT composites, respectively. The maximum ZT value reached 3.05×10^{-4} at 433 K for the binary PTh/MWCNT composite with MWCNT content of 40 wt.%. These results suggest that the thermoelectric performance of PTh/MWCNT composites can be greatly enhanced compared with pure PTh.

Key words: Thermoelectric material, binary PTh/MWCNT composites, ternary PTh/SnSe/MWCNT composites, ZT

INTRODUCTION

Thermoelectric materials, which can enable energy conversion between heat and electricity, have attracted great interest owing to the global energy crisis and the advantages of thermoelectric devices such as their small size, lack of pollution, and no moving parts, and that they are easy to carry.[1–6] The energy conversion efficiency of thermoelectric materials is quantified by the dimensionless figure of merit $ZT = \alpha^2\sigma T/\kappa$, where α is the Seebeck coefficient, σ is the electrical conductivity, κ is the thermal conductivity, and T is absolute temperature. For a given thermoelectric material, the temperature-dependent Seebeck coefficient α is calculated as $\alpha(T) = -\Delta V/\Delta T$, where ΔV is the potential difference and ΔT is the temperature gradient. The sign of α indicates the conduction type, with $\alpha < 0$ for n-type and $\alpha > 0$ for p-type semiconductors.[7] The electrical conductivity σ can be expressed as the product of the charge carrier mobility μ and the charge carrier concentration n: $\sigma = nq\mu$, where q is the electric charge.[8,9] The thermal conductivity κ is determined by the equation $\kappa = \rho DC_p$, where ρ is the density, D is the

(Received October 7, 2019; accepted December 28, 2019; published online January 10, 2020)

thermal diffusivity, and C_p is the specific heat capacity. A high-performance thermoelectric material requires a high Seebeck coefficient and electrical conductivity, but low thermal conductivity.[10–13] However, these three parameters α, σ, and κ exhibit strong interdependence and vary with temperature, which impedes the maximization of ZT, requiring a compromise between them to be found.[14]

Currently, the most popular thermoelectric materials are inorganic materials such as SnSe, Bi_2Te_3, and Zn_4Sb_3, which show better thermoelectric performance.[15–17] In recent decades, nanostructured inorganic materials, in which the thermal conductivity is reduced by phonon scattering at grain boundaries while the Seebeck coefficient is increased without greatly suppressing the electrical conductivity via the energy filtering effect, have shown great improvements in ZT.[18] However, the toxicity of the elements in such inorganic compounds, the scarcity and high cost of the raw materials, the difficulty in the processing, and the high temperature of preparation have seriously limited their wide application. Recently, conducting polymers have attracted much attention as organic thermoelectric materials, since they possess many advantages over inorganic materials, such as low density, facile processability, low cost, plentiful resources, nontoxicity, and adjustable molecular structure.[1,2,4,19] The conducting polymers are mainly conjugated polymers, such as polythiophene (PTh),[20–22] polyaniline (PANI),[23] polypyrrole (PPy),[24] and poly(3,4-ethylenedioxythiophene) (PEDOT).[25–29] They usually possess intrinsic low thermal conductivity. Nevertheless, organic materials have low electrical conductivity and Seebeck coefficient, which result in poor thermoelectric performance compared with inorganic materials. Many efforts have been made to improve the thermoelectric performance of organic materials in recent years; For instance, one approach is to introduce nanostructured inorganic materials with excellent thermoelectric performance into a conducting polymer matrix to form organic/inorganic composites such as PTh/single-walled carbon nanotubes (SWCNT),[30] poly(3-hexylthiophene)(P3HT)/Bi_2Te_3,[14] PEDOT/Sb_2Te_3,[31,32] PANI/carbon nanotubes (CNTs),[23,33] PPy/CNTs,[34] and TiO_2/CNT/PANI.[35] These organic/inorganic composite materials simultaneously exhibit the advantages of both inorganic and organic thermoelectric materials to some extent.

Polythiophene (PTh) and its derivatives in both doped and undoped state have been extensively studied for various applications due to their high electrical conductivity, environment friendliness, good environmental stability, high flexibility, and moderate bandgap.[36] Multiwalled carbon nanotubes and SnSe powders were selected as inorganic materials. Carbon nanotubes (CNTs) have attracted great interest as inorganic fillers and have frequently been used to improve the electrical properties of organic thermoelectric materials because of their unique structure and good electrical and mechanical properties.[20,23,36] SnSe is one of the most promising state-of-the-art inorganic thermoelectric materials because it has ultrahigh Seebeck coefficient and ultralow thermal conductivity.[37–39] In this work, PTh was chosen as the organic material and binary PTh/MWCNT and ternary PTh/SnSe/MWCNT composites with different weight proportions were prepared to study their thermoelectric performance. As expected, the PTh-based composites exhibited much better thermoelectric performance than pure PTh.

EXPERIMENTAL PROCEDURES

Sample Preparation

Thiophene (Th, 99+%) and MWCNTs were purchased from Alfa Aesar. Anhydrous iron(III) chloride ($FeCl_3$, AR) was purchased from Shanghai Meryer Chemical Technology Co. Ltd. Acetonitrile (CH_3CN, AR), n-hexane ($n-C_6H_{14}$, AR), methanol (CH_3OH, AR), ethanol (C_2H_5OH, AR), and sodium hydroxide (NaOH, AR) were bought from Sinopharm Chemical Regent Co. Ltd. Selenium (Se, 99.99%) powder and tin chloride dihydrate ($SnCl_2 \cdot 2H_2O$, 99.99%) were purchased from Aladdin Regent Co. Ltd. Sodium borohydride ($NaBH_4$, AR) was purchased from Shanghai Lingfeng Chemical Regent Co. Ltd. All the above chemicals were used as received, and deionized water (18.2 MΩ) was used throughout the experiment.

PTh microparticles were synthesized at an interface between $n-C_6H_{14}$ and CH_3CN according to the procedure previously reported by Li et al.[40] $FeCl_3$ was used as the oxidant and was dissolved in CH_3CN phase. A typical procedure is as follows: Firstly, 1.5 mL thiophene monomer was dissolved in 50 mL $n-C_6H_{14}$ at room temperature and stirred for 30 min. Secondly, 12.3 g $FeCl_3$ was dissolved in 40 mL of CH_3CN and stirred for 10 min. The molar ratio of thiophene/$FeCl_3$ was 1:4. Thirdly, the $FeCl_3$ solution was slowly added into the prepared $n-C_6H_{14}$ solution with thiophene, then the mixture was consistently stirred at room temperature for 24 h. Fourthly, the PTh microparticles were collected from the polymerization media by centrifugation and further purified with methanol by centrifugation for more than eight times until the upper liquid in the centrifuge tube was colorless to remove the unreacted chemicals. The color of the PTh microparticles changed from dark green to dark red during the washing procedure. Finally, PTh powders were obtained after drying in air for 12 h at 80°C.

Polycrystalline SnSe powders were successfully prepared by hydrothermal method similar to that previously reported by Han et al.[37] The preparation process was as follows: First, 24 g NaOH and 13.53 g $SnCl_2 \cdot 2H_2O$ were dissolved in 300 mL deionized water and gently stirred to obtain

Na_2SnO_2 solution. Second, 4.73 g Se powder and 4.54 g $NaBH_4$ were added into 300 mL deionized water and stirred to obtain transparent NaHSe solution. Third, the Na_2SnO_2 solution was heated until it boiled, then the NaHSe solution prepared in advance was dropped into the Na_2SnO_2 solution, immediately producing black precipitates. Fourth, the mixture was reacted at the boiling temperature for 2 h, then the fabricated products were collected by centrifugation after cooling down to room temperature and washed using deionized water and ethanol for several times. Final, fine SnSe powder was obtained by drying under vacuum for 12 h at 50°C.

Binary PTh/MWCNT and ternary PTh/SnSe/MWCNT composites with different weight proportions, as presented in Table I, were prepared by solution mixing, ultrasonic dispersion, and mechanical ball mixing. Meanwhile, binary 10 wt.%SnSe/90 wt.%MWCNT and ternary 50 wt.%PTh/30 wt.%SnSe/40 wt.%MWCNT composites were also prepared by this method. PTh, MWCNT, and SnSe powders were mixed in a 250-mL round flask with 150 mL anhydrous ethanol. The mixture was stirred for 1 h at room temperature, then ultrasonically dispersed for 30 min and collected by filtering from the solvent and drying under vacuum at 70°C for 24 h. The dried mixtures were ground for 30 min in an agate mortar, then mechanically ball milled in a cylindrical jar. Finally, the ball-milled mixtures were collected by filtering and drying under vacuum at 70°C for 24 h, then the well-dispersed binary PTh/MWCNT and ternary PTh/SnSe/MWCNT composite powders were obtained after milled in an agate mortar for 30 min. In the ternary PTh/SnSe/MWCNT composites, the SnSe content was fixed at 10 wt.%. All the powders were cold pressed into discs with diameter of 15 mm at pressure of 25 MPa for measurement of thermoelectric properties. The uncertainties on the electrical conductivity, thermal conductivity, Seebeck coefficient, and ZT values are ±3%, ±4%, ±5%, and ±11%, respectively.[41]

Table I. Component proportions of PTh/MWCNT and PTh/SnSe/MWCNT composites

Sample	PTh (wt.%)	MWCNT (wt.%)	SnSe (wt.%)
1	100	–	–
B-1	90	10	–
B-2	80	20	–
B-3	70	30	–
B-4	60	40	–
B-5	50	50	–
T-1	80	10	10
T-2	70	20	10
T-3	60	30	10
T-4	50	40	10
T-5	40	50	10

Characterization

Fourier-transform infrared (FT-IR) spectroscopy was conducted on a Nicolet 5700 FT-IR spectrometer with resolution of 4 cm^{-1} in the wavenumber range of 400–4000 cm^{-1}. Powder x-ray diffraction (XRD) patterns of all the composites were obtained on a Bruker D8 Advance x-ray diffractometer with Cu K_α radiation ($\lambda = 1.5418$ Å). The morphology of the PTh, MWCNT, SnSe, and all the composites was observed by field-emission scanning electron microscopy (FESEM). The thermal stability of the materials was studied by thermogravimetric analysis (TGA) on a STA 7300 thermal analysis instrument. The samples were heated from 30°C to 1000°C at a rate of 10 K min^{-1} in nitrogen atmosphere. The electrical conductivity (σ) and Seebeck coefficient (α) of the bulk composites were measured simultaneously from room temperature to 150°C by using a commercial Seebeck coefficient/electrical conductivity measuring system (ZEM-3, ULVAC-RIKO, Inc.) in helium atmosphere. For the pure PTh bulk sample, the electrical conductivity was measured by using the standard four-probe technique with a constant direct current (DC) of 10 μA in vacuum, and the Seebeck coefficient was measured using the comparative method against a standard Constantan (Ni: 40%) reference with known Seebeck coefficient (α). The thermal conductivity (κ) of all the samples was calculated using the relationship $\kappa = \rho D C_p$, where D is the thermal diffusivity obtained by the laser flash diffusivity method (LFA-457, Netzsch, German) in argon atmosphere, C_p is the specific heat capacity measured by differential scanning calorimeter (DSC Q20, TA instrument, USA), and ρ is the density of the material as determined by the Archimedes method.

RESULTS AND DISCUSSION

FT-IR Spectroscopy

The FT-IR spectra of pure PTh, MWCNTs, and the 80 wt.%PTh/20 wt.%MWCNT and ternary PTh/SnSe/MWCNT composites are shown in Fig. 1. In the spectrum of pure PTh, the weak absorption peak at 3060 cm^{-1} can be attributed to C–H stretching vibrations of thiophene ring.[40,42] The wavenumber range of 600 cm^{-1} to 1500 cm^{-1} contains the fingerprint of pure PTh. The peaks at 1488 cm^{-1} and 1436 cm^{-1} can be assigned to C=C symmetric stretching vibrations of thiophene ring.[43] The band at 1320 cm^{-1} is ascribed to C–C stretching vibration. The peaks at 1109 cm^{-1} as well as 1028 cm^{-1} are identified as in-plane bending vibrations of aromatic C–H.[43,44] The strongest absorption peak at 784 cm^{-1} belongs to C–H out-of-plane stretching vibration, indicating α–α linkage between the thiophene rings. The characteristic peak at 693 cm^{-1} is indicative of C–S stretching vibration of thiophene ring.[42–44] The new band at 1737 cm^{-1} may be

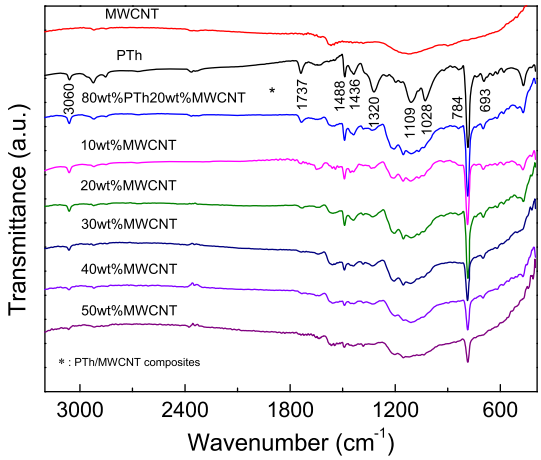

Fig. 1. FT-IR spectra of the pure PTh, MWCNTs, and binary 80 wt.%PTh/20 wt.%MWCNT and ternary PTh/SnSe/MWCNT composites with different weight proportions.

caused by C=C asymmetric stretching vibration of thiophene ring. All these characteristic absorption peaks confirm the polymerization of the PTh microparticles. The binary PTh/MWCNT and ternary PTh/SnSe/MWCNT composites showed FT-IR bands nearly identical to those of PTh in the range of 600 cm^{-1} to 1500 cm^{-1}. However, the intensity of these characteristic peaks gradually weakened with increase of the MWCNT content from 10 wt.% to 50 wt.% for the ternary PTh/SnSe/MWCNT and binary PTh/MWCNT composite samples, and some peaks were even obscured by the absorption bands of the MWCNTs.

x-Ray Diffraction Analysis

Figure 2 presents the x-ray diffraction patterns of pure PTh, MWCNTs, SnSe, and the binary PTh/MWCNT and ternary PTh/SnSe/MWCNT composite samples with different weight proportions. The XRD pattern of pure PTh exhibits a broad, amorphous diffraction peak at approximately $2\theta = 20–24°$, which is in accordance with previous reports.[40,43] The characteristic peaks at approximately $2\theta = 25.7°$, 39°, and 43° belong to pure MWCNT (Fig. 2a), while the peaks at $2\theta = 25.3°$, 29.4°, 30.4°, 31°, 37.8°, 43°, and 49.7° are ascribed to polycrystalline SnSe powder (Fig. 2b), consistent with Joint Committee on Powder Diffraction Standards (JCPDS) card no. 48-1224. Furthermore, a sharp peak appeared at $2\theta = 18°$ for all composites but not pure PTh, which can be attributed to ZrO_2 introduced during ball milling. The diffraction patterns for the binary PTh/MWCNT composite samples contained the characteristic peaks of both PTh and MWCNT, and the intensity of the peaks became stronger with increase of the MWCNT content. In the diffraction patterns of the ternary PTh/SnSe/MWCNT composites, the characteristic peaks of PTh, MWCNT, and SnSe merged, while the intensity of the characteristic peak of MWCNT at $2\theta =$

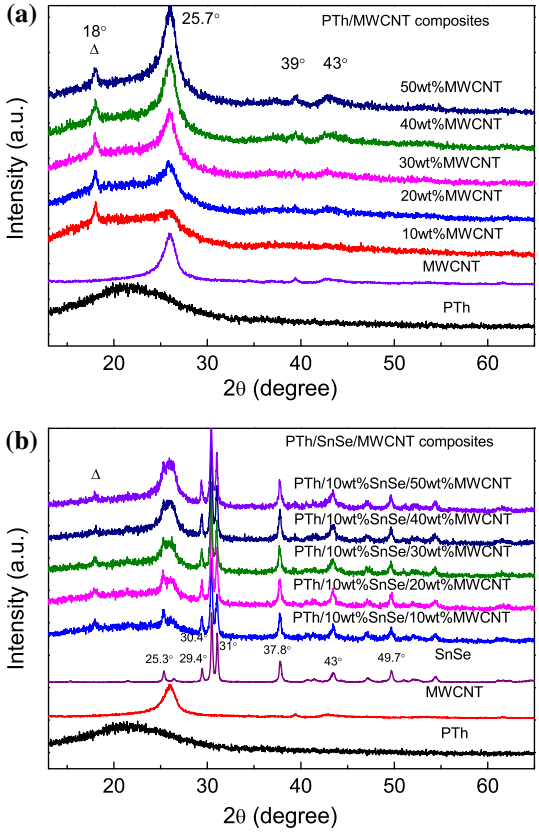

Fig. 2. x-Ray diffraction patterns of (a) pure PTh, MWCNTs, and binary PTh/MWCNT composites, and (b) pure PTh, MWCNTs, SnSe, and ternary PTh/SnSe/MWCNT composites with different MWCNT contents.

25.7° became stronger with increase of the MWCNT content from 10 wt.% to 50 wt.%, overlapping with a peak of SnSe at $2\theta = 25.3°$. These x-ray diffractograms confirm the successful preparation of the binary PTh/MWCNT and ternary PTh/SnSe/MWCNT composites.

FESEM

The microscopic morphology of pure PTh, SnSe, and the binary PTh/MWCNT and ternary PTh/SnSe/MWCNT composites as observed by field-emission scanning electron microscopy (FESEM) is shown in Fig. 3. From Fig. 3a, b, it is clearly observed that the pure PTh sample polymerized at an interface was composed of spherical particles with nearly uniform dispersion. The diameter of the particles was around 160 nm to 200 nm. The SnSe prepared by a hydrothermal method presented laminated structure with a wide size range. Figure 3c–g shows the morphology of the binary PTh/MWCNT composites with different weight proportions. It is obviously seen that the MWCNTs were uniformly dispersed into the PTh microparticle matrix when the MWCNT content was less than 30 wt.%, while the PTh microparticles were covered by MWCNTs when the MWCNT content exceeded 30 wt.%. For the ternary PTh/SnSe/MWCNT

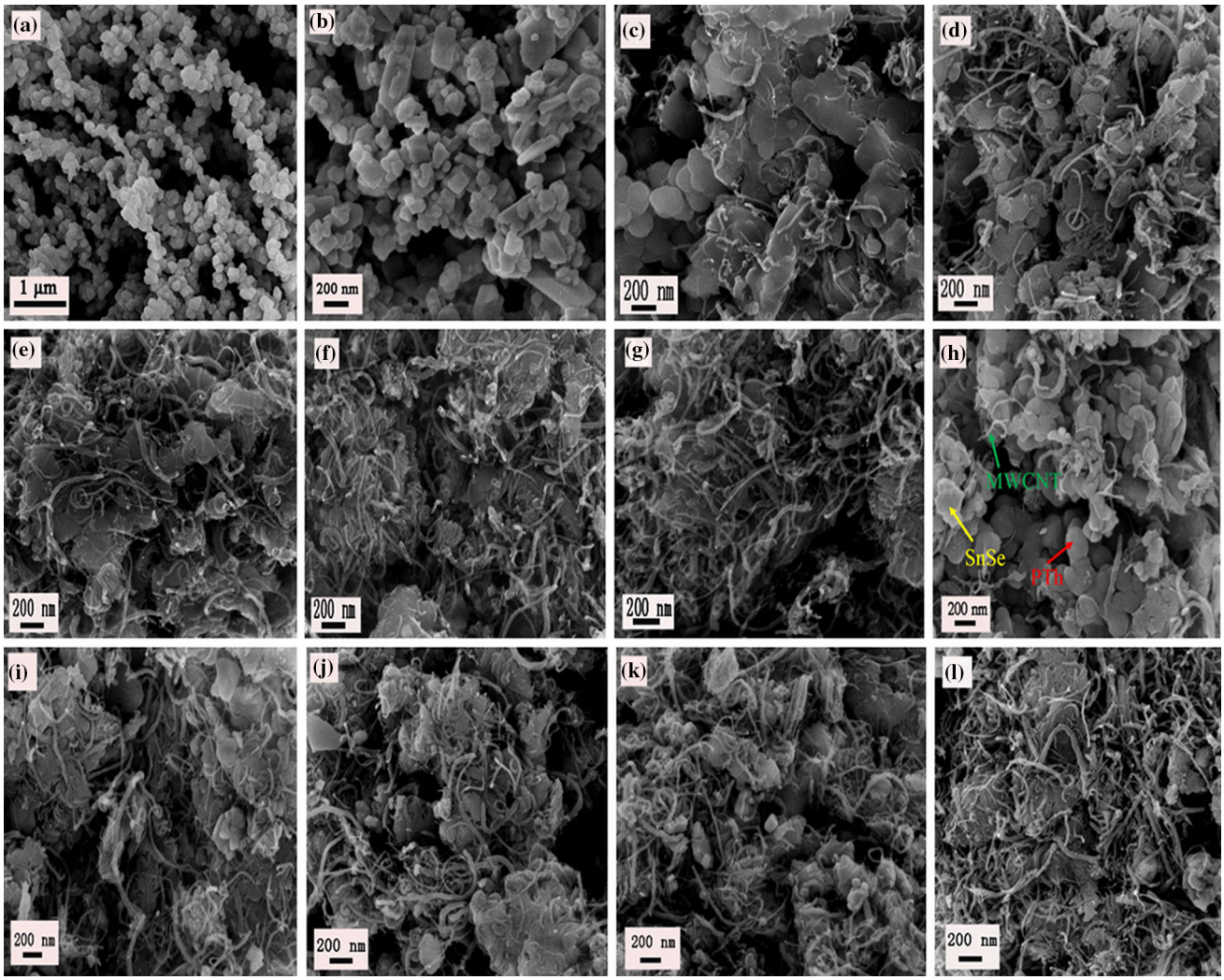

Fig. 3. FESEM images of (a) PTh microparticles, (b) SnSe powder, PTh/MWCNT composites with MWCNT content of (c) 10 wt.%, (d) 20 wt.%, (e) 30 wt.%, (f) 40 wt.%, and (g) 50 wt.%, and PTh/SnSe/MWCNT composites with MWCNT content of (h) 10 wt.%, (i) 20 wt.%, (j) 30 wt.%, (k) 40 wt.%, and (l) 50 wt.%.

composite samples, the morphology is presented in Fig. 3h–l. With increase of the MWCNT content from 10 wt.% to 50 wt.%, the MWCNTs and SnSe were first coated by PTh microparticle matrix, then the morphology changed to wrapping of PTh particles and SnSe by MWCNTs. Layered SnSe could be found in the FESEM images of all the ternary PTh/SnSe/MWCNT composite samples (Fig. 3h–l). The red, yellow, and green arrows in Fig. 3h indicate PTh microparticles, SnSe, and MWCNTs, respectively. These FESEM studies are consistent with the FT-IR spectroscopy and XRD analysis results above, confirming that uniformly dispersed PTh/MWCNT and PTh/SnSe/MWCNT composites were obtained by solution mixing, ultrasonic dispersion, and mechanical ball milling.

In addition, there are two other phenomena which need to be noted. The PTh microparticles tended to aggregate and the particle size increased after ultrasonic dispersion and mechanical ball milling, which is due to the fact that the polymer is prone to deform under external forces. Another phenomenon is that the coating of PTh and SnSe by MWCNTs in the ternary PTh/SnSe/MWCNT composites was more obvious than in the binary PTh/MWCNT composites when the MWCNT content exceeded 40 wt.%, which is due to the lower PTh content in the ternary composites even for given MWCNT content (since the SnSe content was fixed at 10 wt.%).

Thermogravimetric Analysis

The thermal stability of pure PTh and the binary 80 wt.%PTh/20 wt.%MWCNT and ternary PTh/10 wt.%SnSe/50 wt.%MWCNT composites was investigated, and the results are shown in Fig. 4. In the inset to this figure, an obvious weight loss occurs at the same temperature of 700 K for all three samples, being due to the decomposition of PTh. Pure SnSe is reported to be stable up to high

temperature of 993 K,[45] while pure MWCNTs are thermally stable to temperatures above 1000 K.[20,46] Therefore, the rate of mass loss of pure PTh is faster than that of the composites. The thermal stability of the binary 80 wt.%PTh/20 wt.%MWCNT and ternary PTh/10 wt.%SnSe/50 wt.%MWCNT composite samples was better than that of pure PTh below 500 K, with mass loss of less than 1%, which can be attributed to the good thermal stability of both the MWCNTs and SnSe and the uniform dispersion of the three components. These results suggest that the thermoelectric properties of pure PTh and the binary PTh/MWCNT and ternary PTh/SnSe/MWCNT composites can be measured up to 500 K without destroying the molecular structure of the polymer.

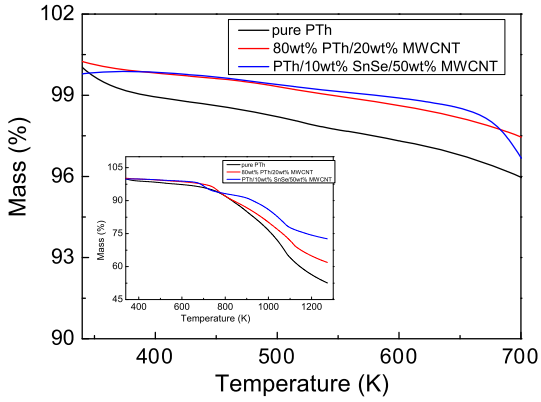

Fig. 4. TGA results for pure PTh and binary 80 wt.%PTh/20 wt.%MWCNT and ternary PTh/10 wt.%SnSe/50 wt.%MWCNT composites between 340 K and 700 K. Inset: TGA curves of the three samples between 340 K and 1273 K.

Thermoelectric Properties

Binary PTh/MWCNT Composites

Figure 5a, b, c, and d present the electrical conductivity σ, Seebeck coefficient α, thermal conductivity κ, and ZT value of the pure PTh microparticles and binary PTh/MWCNT composite samples in the temperature range of 303 K to 430 K. Meanwhile, the thermoelectric properties of pure MWCNT were also measured for comparison with the PTh/MWCNT composites (Supplementary Fig. S1). The pure PTh microparticles showed ultralow electrical conductivity, which increased from 0.0211 Sm^{-1} at 303 K to 0.334 Sm^{-1} at 430 K, revealing a semiconducting characteristic. In comparison with pure PTh, the electrical conductivity of the binary PTh/MWCNT composites increased rapidly with increase of the MWCNT content. At room temperature, the electrical conductivity was 61.3 Sm^{-1} for the binary 90 wt.%PTh/10 wt.%MWCNT composite, increasing to 1035.6 Sm^{-1} for the binary 50 wt.%PTh/50 wt.%MWCNT composite. Meanwhile, the

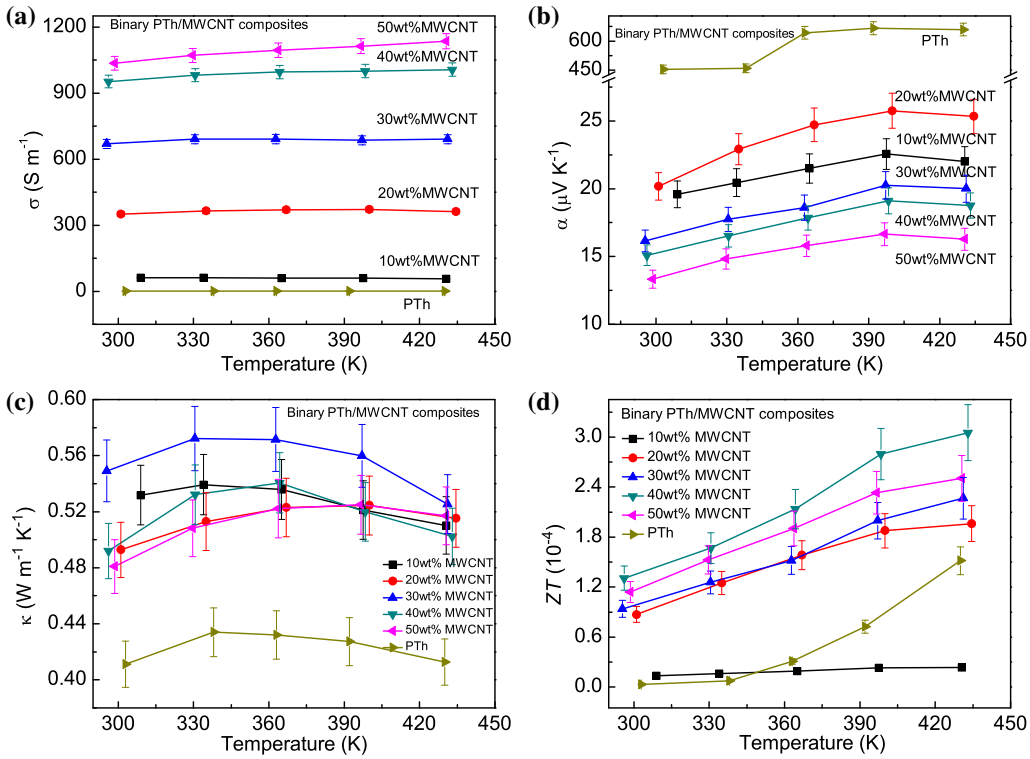

Fig. 5. Thermoelectric properties of pure PTh and binary PTh/MWCNT composite samples: (a) electrical conductivity σ, (b) Seebeck coefficient α, (c) thermal conductivity κ, and (d) ZT value.

electrical conductivity of all the composite samples increased slowly with temperature from room temperature to 430 K.

As shown in Fig. 5b, the Seebeck coefficient of pure PTh and the binary PTh/MWCNT composites was positive in each case, indicating that pure PTh and the binary PTh/MWCNT composites were *p*-type semiconductors. Ultrahigh Seebeck coefficients of 450 μV K^{-1} to 650 μVK^{-1} were obtained for pure PTh. However, the Seebeck coefficient decreased sharply after introducing MWCNTs in the binary PTh/MWCNT composites. For the binary 50 wt.%PTh/50 wt.%MWCNT composite, α decreased to a minimum value of 13.3 μVK^{-1} at room temperature. This might be due to the increase of the carrier concentration introduced by the MWCNTs. On the other hand, the Seebeck coefficient of pure MWCNT was also rather low, being only $-2.8\,\mu$VK^{-1} at room temperature (Supplementary Fig. S1).

The thermal conductivity κ of pure PTh and the binary PTh/MWCNT composite samples is shown in Fig. 5c. The C_p, D, and ρ values of PTh and the binary composites are shown in Supplementary Fig. S2 and Table S1, respectively. Pure PTh showed an ultralow thermal conductivity of 0.41 Wm^{-1} K^{-1} at room temperature, first showing an increase with increasing temperature, reaching a maximum value, then decreasing with temperature. In comparison with pure PTh, higher thermal conductivity was observed for all the binary PTh/MWCNT composites, albeit below 0.6 Wm^{-1} K^{-1}. This indicates that the thermal conductivity of the PTh/MWCNT composites was less affected by the inclusion of MWCNTs. The low thermal conductivity of all the PTh/MWCNT composites can be attributed to strong phonon scattering at the interfaces between PTh and MWCNTs which exist in these composite materials. The variation of the thermal conductivity with temperature in the binary PTh/MWCNT composites was similar to that of pure PTh.

Using the above measured parameters, the *ZT* value of pure PTh was calculated to be 0.032×10^{-4} at 303 K, increasing to 1.52×10^{-4} at 430 K due to the higher Seebeck coefficient and electrical conductivity at high temperatures. The *ZT* values of all the PTh/MWCNT composites were higher than that of pure PTh at room temperature, increasing from 0.13×10^{-4} to 1.3×10^{-4} as the MWCNT content was increased from 10 wt.% to 40 wt.%. Thus, the thermoelectric performance of the PTh/MWCNT composites was enhanced by nearly two orders of magnitude compared with pure PTh at room temperature. The maximum *ZT* reached 3.05×10^{-4} at 433 K for the binary PTh/MWCNT composite with MWCNT content of 40 wt.%.

Ternary PTh/SnSe/MWCNT Composites

Figure 6 shows the thermoelectric properties of the ternary PTh/SnSe/MWCNT composite samples in the temperature range from room temperature ($\sim$ 300 K) to 430 K. The results for pure PTh are also shown for comparison. Furthermore, the thermoelectric properties of the 10 wt.%SnSe/90 wt.%MWCNT composite were also measured for comparison with the PTh/SnSe/MWCNT composites (Supplementary Fig. S1). The ternary PTh/SnSe/MWCNT composite samples exhibited much higher electrical conductivity compared with pure PTh, and their conductivity was also higher than that of the binary PTh/MWCNT composites with identical MWCNT content, which can be ascribed to the addition of SnSe with high electrical conductivity. The conductivity increased continuously with increase of the MWCNT content from 10 wt.% to 50 wt.%, reaching 1221.9 Sm^{-1} at room temperature for the ternary PTh/10 wt.%SnSe/50 wt.%MWCNT composite. Additionally, the electrical conductivity of all the composite samples showed a slight increase with increasing temperature, indicating semiconducting behavior.

Figure 6b presents the Seebeck coefficient of PTh and the PTh/SnSe/MWCNT composites. Similar to the binary PTh/MWCNT composites, the ternary PTh/SnSe/MWCNT composites also exhibited much lower Seebeck coefficient compared with pure PTh across the whole measurement temperature range. At room temperature, the maximum Seebeck coefficient was found to be 15.9 μVK^{-1} for the MWCNT content of 30 wt.%, while in the PTh/SnSe/MWCNT composite with MWCNT content of 50 wt.%, it showed a minimum value of 12.9 μVK^{-1}, revealing an irregular change with increase of the MWCNT content. This can be ascribed to the complex synergistic mechanism caused by the coexistence of three phases in these composite materials.

The thermal conductivity of pure PTh and the ternary PTh/SnSe/MWCNT composite samples is shown in Fig. 6c. The C_p, D, and ρ values of the ternary composites are shown in Supplementary Fig. S3 and Table S1, respectively. The ternary PTh/SnSe/MWCNT composites showed higher thermal conductivity compared with PTh, but all below 0.59 Wm^{-1} K^{-1}, indicating that dispersion of SnSe and MWCNTs into PTh had only a very slight effect on the thermal conductivity. The thermal conductivity of the PTh/SnSe/MWCNT composite with 20 wt.% MWCNT was the highest at 360 K and 390 K, which might be due to the uniform dispersion of MWCNTs in PTh and its higher bulk density than the other ternary composites. FESEM revealed that the MWCNTs were uniformly dispersed into the PTh microparticle matrix when the MWCNT content was less than 30 wt.%. The thermal

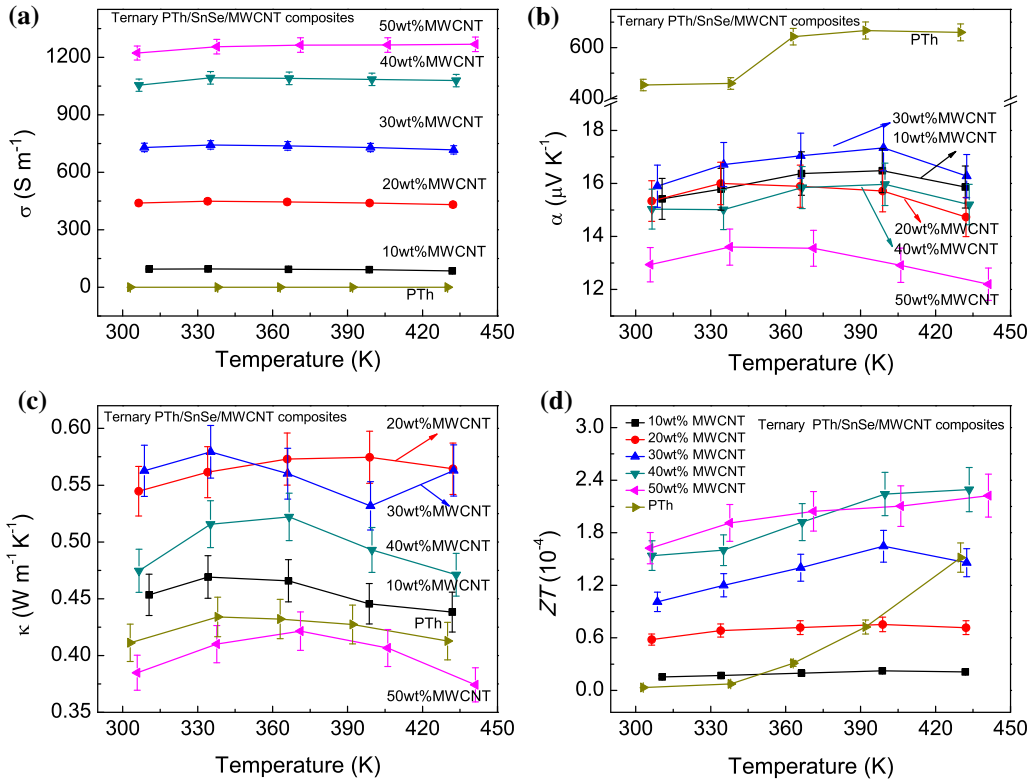

Fig. 6. Thermoelectric properties of pure PTh and ternary PTh/SnSe/MWCNT composite samples: (a) electrical conductivity σ, (b) Seebeck coefficient α, (c) thermal conductivity κ, and (d) ZT value.

conductivity of SnSe single crystals exhibits anisotropy, depending on the crystallographic axis ($\sim$ 0.46 W m^{-1} K^{-1}, 0.70 W m^{-1} K^{-1}, and 0.68 Wm^{-1} K^{-1} at room temperature along a, b, and c axis, respectively).[38] In our SnSe nanopowder, the average thermal conductivity should be close to or just slightly higher than that of pure PTh. The low thermal conductivity of the ternary PTh/SnSe/MWCNT composites might also be due to strong phonon scattering taking place at various interfaces in the composites. The thermal conductivity became even lower than that of pure PTh when the MWCNT content was increased to 50 wt.%, which might be caused by the lower material density, thermal diffusivity, or specific heat capacity of the ternary PTh-based composite samples compared with pure PTh.

The temperature dependence of the ZT value of the ternary PTh/SnSe/MWCNT composite samples is shown in Fig. 6d. Similar to the binary PTh/MWCNT composite materials, the ZT value of all the PTh/SnSe/MWCNT composite samples was higher than that of pure PTh at room temperature, increasing to a value of 1.62×10^{-4} at room temperature when the MWCNT content was 50 wt.%, which is higher than that of the binary PTh/MWCNT composites (1.3×10^{-4}) or 10 wt.%SnSe/90 wt.%MWCNT composite (0.11×10^{-4}) at room temperature. This illustrates that the ternary organic/inorganic composites exhibited better thermoelectric performance than the binary ones to some extent.[35] The maximum ZT reached 2.3×10^{-4} at 433.5 K for ternary PTh/SnSe/MWCNT composites, being lower than that of the binary PTh/MWCNT composites (3.05×10^{-4} at 433 K).

These results confirm that introduction of MWCNTs or SnSe/MWCNTs into PTh can greatly improve the thermoelectric performance of pure PTh. We further prepared the ternary 50 wt.%PTh/30 wt.%SnSe/40 wt.%MWCNT composite to study whether the content of SnSe affected the performance of the ternary PTh/SnSe/MWCNT composites and compare it with the ternary 50 wt.%PTh/10 wt.%SnSe/40 wt.%MWCNT composite, which exhibited the best thermoelectric performance at high temperature among the ternary PTh/SnSe/MWCNT composites. The thermoelectric properties of the ternary 50 wt.%PTh/30 wt.%SnSe/40 wt.%MWCNT composite is shown in Supplementary Fig. S4. It is clearly seen that the σ, α, and ZT values of the ternary 50 wt.%PTh/30 wt.%SnSe/40 wt.%MWCNT composite were much lower than those of the ternary 50 wt.%PTh/10 wt.%SnSe/40 wt.%MWCNT composite, indicating that the thermoelectric performance of the ternary composites will sharply decrease with increase of the SnSe

Table II. Comparison of thermoelectric properties of PTh/MWCNT-based composites at 120°C

PTh/CNT Composite	Methods	σ (Sm^{-1})	α (μVK^{-1})	κ (Wm^{-1}K^{-1})	*ZT*	Ref.
PTh/SWCNT	*In situ* polymerization	41 (RT)	–	–	–	30
PTh/MWCNT (40 wt.%)	Ball milling	~ 338	~ 16.4	~ 0.54	0.67×10^{-4}	47
PTh/MWCNT (40 wt.%)	Solution mixing	~ 348	~ 25.6	~ 0.57	1.57×10^{-4}	48
PTh/MWCNT (40 wt.%)	Ball milling	999	19.1	0.52	2.79×10^{-4}	This work
PTh/SnSe/MWCNT (40 wt.%)	Ball milling	1085	15.9	0.49	2.24×10^{-4}	This work

content. Therefore, introduction of only a small amount of SnSe can enhance the thermoelectric performance.

Table II presents the thermoelectric properties at 120°C of various PTh/MWCNT-based composites reported by other workers in recent years, clearly revealing that the composites described herein exhibited better thermoelectric performance. Furthermore, it is clear that the electrical conductivity rapidly increased with increasing MWCNT content in both the binary PTh/MWCNT and ternary PTh/SnSe/MWCNT composites, while the Seebeck coefficient and thermal conductivity showed no obvious change. It is therefore expected that the *ZT* value could be further enhanced by improving the electrical conductivity via increasing the MWCNT content.

CONCLUSIONS

Binary PTh/MWCNT and ternary PTh/SnSe/MWCNT composites were prepared by solution mixing, ultrasonic dispersion, and mechanical ball milling. FESEM revealed SnSe and MWCNTs well dispersed into a PTh microparticle matrix when the MWCNT content was lower than 30 wt.%, while PTh and SnSe were wrapped by a MWCNT matrix on further increase of the MWCNT content. The thermal stability of the composites was better than that of pure PTh according to TGA. The electrical conductivity of both the binary PTh/MWCNT and ternary PTh/SnSe/MWCNT composites was greatly improved compared with pure PTh across the whole measurement temperature range. However, the Seebeck coefficient decreased dramatically after introducing SnSe and MWCNTs into PTh. The thermal conductivity remained below 0.6 Wm^{-1}K^{-1} for all the composites. As a result, the *ZT* values of all the composites were significantly enhanced compared with pure PTh. At room temperature, the maximum *ZT* value reached 1.3×10^{-4} and 1.62×10^{-4} for the binary PTh/MWCNT and ternary PTh/SnSe/MWCNT composites, being about 40 and 50 times that of pure PTh, respectively. These results show that organic/inorganic composites can effectively improve the thermoelectric performance compared with pure conducting polymers.

ACKNOWLEDGMENTS

This work was supported by the National Natural Science Foundation of China under Grant Nos. 11575131, 11775163, and 11875208, and the Natural Science Foundation of Hubei Province under Grant No. 2016CFA080.

CONFLICT OF INTEREST

There are no conflicts of interest to declare.

ELECTRONIC SUPPLEMENTARY MATERIAL

The online version of this article (https://doi.org/10.1007/s11664-019-07935-8) contains supplementary material, which is available to authorized users.

REFERENCES

1. M. He, F. Qiu, and Z. Lin, *Energy Environ. Sci.* 6, 1352 (2013).
2. B. Russ, A. Glaudell, J.J. Urban, M.L. Chabinyc, and R.A. Segalman, *Nat. Rev. Mater.* 1, 16050 (2016).
3. H. Yao, Z. Fan, H. Cheng, X. Guan, C. Wang, K. Sun, and J. Ouyang, *Macromol. Rapid Commun.* 39, 1700727 (2018).
4. B.T. McGrail, A. Sehirlioglu, and E. Pentzer, *Angew. Chem. Int. Ed.* 54, 1710 (2015).
5. Y. Li, Y. Du, Y. Dou, K. Cai, and J. Xu, *Synth. Met.* 226, 119 (2017).
6. G.H. Kim, L. Shao, K. Zhang, and K.P. Pipe, *Nat. Mater.* 12, 719 (2013).
7. R. Kroon, D.A. Mengistie, D. Kiefer, J. Hynynen, J.D. Ryan, L. Yu, and C. Muller, *Chem. Soc. Rev.* 45, 6147 (2016).
8. N. Toshima, *Synth. Met.* 225, 3–21 (2017).
9. A.M. Glaudell, J.E. Cochran, S.N. Patel, and M.L. Chabinyc, *Adv. Energy Mater.* 5, 1401072 (2015).
10. J. Zhao, D. Tan, and G. Chen, *J. Mater. Chem. C* 5, 47 (2017).
11. X. Hu, G. Chen, X. Wang, and H. Wang, *J. Mater. Chem. A* 3, 20896 (2015).
12. H. Ju, D. Park, and J. Kim, *Chem. Eng. J* 356, 950 (2019).
13. Y. Li, F. Li, J. Dong, Z. Ge, F. Kang, J. He, H. Du, B. Li, and J.-F. Li, *J. Mater. Chem. C* 4, 2047 (2016).
14. M. He, J. Ge, Z. Lin, X. Feng, X. Wang, H. Lu, Y. Yang, and F. Qiu, *Energy Environ. Sci.* 5, 8351 (2012).
15. C. Chang, M. Wu, D. He, Y. Pei, C.F. Wu, X. Wu, H. Yu, F. Zhu, K. Wang, Y. Chen, L. Huang, J.F. Li, J. He, and L.D. Zhao, *Science* 360, 778 (2018).

16. T. Zhang, K. Zhou, and Z.Q. Chen, *Phys. Status Solidi B* 252, 2179 (2015).
17. H.F. He, X.F. Li, Z.Q. Chen, Y. Zheng, D.W. Yang, and X.F. Tang, *J. Phys. Chem. C* 118, 22389 (2014).
18. X. Zhang and L.-D. Zhao, *J. Materiomics* 1, 92 (2015).
19. H. Wang and C. Yu, *Joule* 3, 53 (2019).
20. Y. Du, S.Z. Shen, W.D. Yang, K.F. Cai, and P.S. Casey, *Synth. Met.* 162, 375 (2012).
21. C. Lai, J. Li, C. Pan, L. Wang, and X. Bai, *J. Electron. Mater.* 45, 5246 (2016).
22. K. Hiraishi, A. Masuhara, H. Nakanishi, H. Oikawa, and Y. Shinohara, *Jpn. J. Appl. Phys.* 48, 071501 (2009).
23. J. Liu, J. Sun, and L. Gao, *Nanoscale* 3, 3616–3619 (2011).
24. L. Fan and X. Xu, *RSC Adv.* 5, 78104 (2015).
25. M. Famili, I.M. Grace, Q. Al-Galiby, H. Sadeghi, and C.J. Lambert, *Adv. Funct. Mater.* 28, 1703135 (2018).
26. B. Zhang, K. Wang, D. Li, and X. Cui, *RSC Adv.* 5, 33885 (2015).
27. G.-H. Kim, J. Kim, and K.P. Pipe, *Appl. Phys. Lett.* 108, 093301 (2016).
28. O. Bubnova, Z.U. Khan, A. Malti, S. Braun, M. Fahlman, M. Berggren, and X. Crispin, *Nat. Mater.* 10, 429 (2011).
29. K. Wei, T. Stedman, Z.-H. Ge, L.M. Woods, and G.S. Nolas, *Appl. Phys. Lett.* 107, 153301 (2015).
30. M.R. Karim, C.J. Lee, and M.S. Lee, *J. Polym. Sci. A Polym. Chem.* 44, 5283 (2006).
31. W. Zheng, P. Bi, H. Kang, W. Wei, F. Liu, J. Shi, L. Peng, Z. Wang, and R. Xiong, *Appl. Phys. Lett.* 105, 023901 (2014).
32. H. Wang, J.-H. Hsu, S.-I. Yi, S.L. Kim, K. Choi, G. Yang, and C. Yu, *Adv. Mater.* 27, 6855 (2015).
33. H. Wang, S.-I. Yi, X. Pu, and C. Yu, *ACS Appl. Mater. Interfaces* 7, 9589 (2015).
34. L. Liang, C. Gao, G. Chen, and C.-Y. Guo, *J. Mater. Chem. C* 4, 526 (2016).
35. F. Erden, H. Li, X. Wang, F. Wang, and C. He, *Phys. Chem. Chem. Phys.* 20, 9411 (2018).
36. T.P. Kaloni, P.K. Giesbrecht, G. Schreckenbach, and M.S. Freund, *Chem. Mater.* 29, 10248 (2017).
37. G. Han, S.R. Popuri, H.F. Greer, J.W. Bos, W. Zhou, A.R. Knox, A. Montecucco, J. Siviter, E.A. Man, M. Macauley, D.J. Paul, W.G. Li, M.C. Paul, M. Gao, T. Sweet, R. Freer, F. Azough, H. Baig, N. Sellami, T.K. Mallick, and D.H. Gregory, *Angew. Chem. Int. Ed.* 55, 6433 (2016).
38. L.D. Zhao, S.H. Lo, Y. Zhang, H. Sun, G. Tan, C. Uher, and C. Wolverton, *Nature* 508, 373 (2014).
39. L.D. Zhao, G. Tan, S. Hao, J. He, Y. Pei, H. Chi, H. Wang, S. Gong, H. Xu, V.P. Dravid, C. Uher, G.J. Snyder, C. Wolverton, and M.G. Kanatzidis, *Science* 351, 141 (2016).
40. X.G. Li, J. Li, Q.K. Meng, and M.R. Huang, *J. Phys. Chem. B* 113, 9718 (2009).
41. X. She, X. Su, H. Xie, J. Fu, Y. Yan, W. Liu, P.F. Poudeu Poudeu, and X. Tang, *ACS Appl. Mater. Interfaces* 10, 25519 (2018).
42. M.R. Karim, K.T. Lim, C.J. Lee, and M.S. Lee, *Synth. Met.* 157, 1008 (2007).
43. M.-D. Lu and S.-M. Yang, *Synth. Met.* 154, 73 (2005).
44. X.G. Li, J. Li, and M.R. Huang, *Chemistry* 15, 6446 (2009).
45. A. Agarwal, S.H. Chaki, and D. Lakshminarayana, *Mater. Lett.* 61, 5188 (2007).
46. S. Mallakpour, A. Abdolmaleki, and S. Borandeh, *Prog. Org. Coat.* 77, 1966 (2004).
47. D. Wang, L. Wang, W. Wang, X. Bai, and J. Li, in *Third International Conference on Smart Materials and Nanotechnology in Engineering* (2012).
48. L. Wang, X. Jia, D. Wang, G. Zhu, and J. Li, *Synth. Met.* 181, 79 (2013).